



# A model to interpret driftwood transport in the Arctic

Quentin Dalaiden<sup>\*</sup>, Hugues Goosse, Olivier Lecomte, David Docquier

Université catholique de Louvain (UCL), Earth and Life Institute (ELI), Georges Lemaître Centre for Earth and Climate Research (TECLIM), Place Louis Pasteur, B-1348 Louvain-la-Neuve, Belgium

## ARTICLE INFO

### Article history:

Received 7 December 2017

Received in revised form

27 April 2018

Accepted 2 May 2018

### Keywords:

Driftwood

Proxy system models

Reconstruction

Holocene

Sea ice

Arctic ocean

## ABSTRACT

Driftwood is frequently used to estimate past changes of sea ice extent and circulation in the Arctic. Nevertheless, driftwood observations are difficult to interpret because of the potentially complex relation with climate change. In order to determine the origin of the observed changes, we built a driftwood transport model (DTM) simulating the driftwood trajectories from the boreal forest to Arctic coasts. The model is driven by three main variables, which are the sea ice velocity, concentration and the sea surface current velocity that can be derived from observations or climate model outputs (e.g. from a General Climate Model – GCM). Overall, the DTM model agrees with the observations, although this comparison needs to be taken with caution because of the sparse data and the uncertainties of driftwood provenance. Through simulations performed with the DTM model, we confirm the strong influence of the variability of the atmospheric circulation on the spatial driftwood distribution. Model simulations of the Mid-Holocene period driven by six GCMs show that small local changes in sea ice circulation – a westward shift in the Transpolar Drift and a reduced Beaufort Gyre during the Mid-Holocene compared to the present period – suffice to explain the driftwood landing change during the Mid-Holocene, with a non-negligible contribution from reduced sea ice concentration. Consequently, a change in driftwood deposit should not be directly interpreted as large modifications in atmospheric circulation and the complexity of the response of driftwood trajectories to past climate changes clearly highlights the interest of using a model to interpret driftwood records.

© 2018 Elsevier Ltd. All rights reserved.

## 1. Introduction

Driftwood represents a unique record that can provide information on sea ice state over several millennia (Hellmann et al., 2017; Funder et al., 2011; Nixon et al., 2016; Dyke et al., 1997). Driftwood from boreal (Canadian and Siberian) forests enters in the Arctic Ocean via river systems because of natural processes such as shoreline erosion or storms. For Siberia, timber originating from industrial activities is also currently an important source of driftwood (Eggertsson, 1993; Hellmann et al., 2013). The woods transported to the Arctic Ocean are trapped into sea ice and then follow sea ice drift. Driftwood can then be transported on long distances before being deposited on Arctic coasts.

The Siberian driftwood is directly transported by the Transpolar

Drift (TPD) – a strong current from the Siberian coasts to Fram Strait and later along the eastern coasts of Greenland. The Canadian driftwood is generally incorporated into the Beaufort gyre (BG) – an anticyclonic circulation located north of the Beaufort sea – before reaching the TPD. The journey of Canadian driftwood across the Arctic is therefore 6–7 years long while the minimum duration of Siberian driftwood transport is 2–3 years (Rigor et al., 2002; Funder et al., 2011). However, the speed and direction of sea ice drift are not the only elements to take into account. Sea ice melting and reduced ice extent play also a large role in the driftwood transport as once driftwood is released from sea ice, it becomes waterlogged and eventually sinks far from the shores (Eggertsson, 1993; Häggblom, 1982). Driftwood transport across the Arctic is thus several years long and driftwood is an indicator of the presence of the multiyear pack sea ice (sea ice that is several years old; Funder et al., 2011; Dyke et al., 1997).

It seems well established that the main source of driftwood found on the Arctic coasts is presently the Siberian forests (Eggertsson, 1993, 1994; Hellmann et al., 2013, 2017, 2015). The first reason is that the voyage from Canada is more precarious because

Abbreviations: General Climate Model, (GCM); Proxy system model, (PSM); Driftwood transport model, (DTM); Beaufort Gyre, (BG); Transpolar Drift, (TPD); Mid-Holocene, (MH); North Atlantic Oscillation, (NAO).

<sup>\*</sup> Corresponding author.

E-mail address: [quentin.dalaiden@uclouvain.be](mailto:quentin.dalaiden@uclouvain.be) (Q. Dalaiden).

the Canadian driftwood must make a detour in BG before reaching the TPD, increasing the probability to sink in the Arctic Ocean (Funder et al., 2011). Furthermore, a larger amount of driftwood comes from the Siberian rivers (compared to Canadian rivers) because of a significant loss of industrial timber (Eggertsson, 1993; Hellmann et al., 2016). Driftwood is found in many locations in the Arctic but observations show that four different regions display the highest occurrence: Ellesmere Island, Greenland, Svalbard and Iceland (Hellmann et al., 2017). Driftwood of Siberian origin dominates in all regions but Greenland (England et al., 2007; Hellmann et al., 2017; Eggertsson, 1993; Funder et al., 2011). Assigning a specific source for each driftwood is complicated as some tree species are present both on Siberian and Canadian sides (Hellmann et al., 2017). Detailed analyses of macroscopy and microscopy, driftwood anatomy and species composition allow a decrease in the driftwood origin uncertainties (Hellmann et al., 2013; Hole and Macias-Fauria, 2017). Moreover, the driftwood sampling is not usually often representative of the total amount deposited in each region because of: the use of driftwood by the local population (Alix, 2005; Wheeler and Alix, 2004), wood decay caused by fungal colonisation making difficult the species determination (Hellmann et al., 2013) and heterogeneous geographic coverage of sampling. Furthermore, the lack of driftwood deposit can be interpreted as the presence of perennial landfast sea ice preventing driftwood from being released on the shore (Kelly and Bennike, 1992; Hole and Macias-Fauria, 2017; Funder et al., 2011). Observations of driftwood deposit have been used to reconstruct changes in sea ice extent and circulation in the Arctic over several thousand years (Hole and Macias-Fauria, 2017; Funder et al., 2011; Bennike, 2004; Dyke et al., 1997). Nevertheless, because of the complex interpretation of the driftwood observations, the available information is often qualitative.

One additional difficulty is that driftwood transport is influenced by both changes in sea ice circulation and concentration. Such a complex dependence is standard in palaeoclimatology. Generally, the climatic variables (sea ice velocity and concentration in our study) can be derived from observations (driftwood occurrence and position in our analysis) using an inverse procedure (e.g. Sachs et al., 1977; Evans et al., 2013). Nevertheless, the inverse procedure may be ill-conditioned because of the multi-variate and non-linear nature of the link between paleoclimatic observations and the climatic variables of interest (Evans et al., 2013; Dee et al., 2015).

An alternative solution is to use a proxy system model (PSM) which predicts the measured quantity on the basis of our current understanding of the processes that lead to the observations and estimates the climatic or environmental forcings (Evans et al., 2013; Dee et al., 2015). In other words, a PSM transposes in a mathematical program the mechanical processes by which climate information is recorded and then observed in the archives (Dee et al., 2015). PSMs improve the interpretation of the signal recorded in archives and isolate the contribution of individual processes in the sensor response. Furthermore, PSMs facilitate the comparison of model results to observations by simulating the directly observed variable using climate model results as inputs. This approach is currently developed for several archives including speleothems, ice cores and woods (e.g. Evans et al., 2013; Dee et al., 2015).

In this study, we propose a PSM for the driftwood transported by sea ice. The model is designed to study the influence of thermodynamic and dynamic changes on driftwood deposits. The next section presents the driftwood transport model (DTM). This first part is accompanied by a short evaluation of fields used to drive the DTM model. The experiments performed with the DTM model are described in section 3. Then, in section 4, two applications of the DTM model are presented. The first application consists in the study of the impact of a change in the atmospheric circulation on

the driftwood distribution. In the second application, the DTM is driven by the results of six climate models for the mid-Holocene in order to improve our understanding of past sea ice changes and to illustrate from a practical example the interest of the approach.

## 2. Model description

### 2.1. Transport model

The main equation of the driftwood transport model (DTM) is

$$\mathbf{v}_i(t) = \frac{d\mathbf{x}_i(t)}{dt} \quad (1)$$

$\mathbf{x}$  and  $\mathbf{v}$  are the position and velocity of each simulated wood ( $i$  ranging 1 to  $n$ , the total number of simulated woods), respectively.  $t$  is the time. Equation (1) is discretised using the forward Euler method:

$$\mathbf{x}_i(t + 1) = \mathbf{x}_i + \mathbf{v}_i(t) \times \Delta t \quad (2)$$

The model time step  $\Delta t$  is one day. As long as sea ice concentration is higher than a threshold (referred to as  $ice_{thr}$  in the DTM model), woods drift with sea ice (driftwood velocity is equal to sea ice velocity). When sea ice concentration is lower than the threshold, woods follow the ocean surface currents (driftwood velocity is equal to the ocean surface velocity) for a limited duration equal to the  $ice_{time}$  parameter before woods sink (Eggertsson, 1993).

The DTM model can be driven by the sea ice velocity and ocean currents derived from large-scale models. However, those present large biases in sea ice velocity near the shores because of their coarse resolution which does not allow a correct representation of the coastal processes. The local processes related to small scale circulation, tides, the landfast ice that blocks the driftwood beaching (Wadhams, 2000), etc., which contribute to the trapping of woods by the ice and to their release on the coast, are not represented in the simulated trajectories. In order to remove this bias in sea ice velocity due to coastal processes, the coastal regions are not explicitly included in the DTM model. Woods are assumed to be released at a prescribed distance from the coast and be deposited on the coast when they are actually at some distance from it (referred to as  $coast_{thr}$  in the DTM model). After calibration tests, we have chosen the effective depart zone as a 100 km band located 300 km from the coast. Within this band, the initial driftwood positions are randomly generated due to the high uncertainty in these positions.

Only "active" driftwood is retained in the simulations. A driftwood is active when it does not go directly back to land (typically when the winds are blowing towards the shore). Moreover, if the distance between the initial and arrival positions is too small (1000 km), driftwood is not taken into account since it is not linked to large-scale sea ice patterns but local processes (Hole and Macias-Fauria, 2017).

The DTM model includes three main parameters for which values are uncertain and difficult to estimate from observations, namely  $coast_{thr}$ ,  $ice_{thr}$  and  $ice_{time}$ . To select adequate values of these parameters, we have performed simulations with the DTM model driven by the outputs of the NEMO-LIM sea ice model (Nucleus for European Modelling of the Ocean and Louvain-la-Neuve sea Ice Model; Barthélemy et al., 2015; see section 2.2) varying each of these parameters in a reasonable range ( $coast_{thr}$ : 75 km and 150 km;  $ice_{thr}$ : 5%, 10%, 15% and 25%;  $ice_{time}$ : 15 days and 45 days; see Table A1 for the details of the calibration simulations). Compared with Eggertsson (1993), the tested values for the  $ice_{time}$  parameter are relatively small as the transport duration of the wood from the continent to the open ocean and the drift duration before the beaching are not taken into account.

Figure A1 represents the driftwood proportions for each arrival coast (South Greenland, North Greenland, Iceland, Svalbard and Ellesmere Island) for the 12 calibration simulations. Figures A2 and A3 show the initial and final positions of simulated woods from each calibration simulation. Since Siberian driftwood landing is common in North Greenland (Funder et al., 2011; Hole and Macias-Fauria, 2017; Hellmann et al., 2017), simulations characterised by a weak driftwood deposit in this region are excluded (simulations 1, 2, 3, 7, 8 and 9). Otherwise, these simulations for which the  $coast_{thr}$  is equal to 75 km show driftwood landing in the southern part of South Greenland (Fig. A2) which does not agree with driftwood observations (Hellmann et al., 2013, 2017). The results of the other simulations are close to each other but we chose the simulation for which the driftwood deposit is the largest in Iceland in order to match at best with the driftwood records (Hellmann et al., 2017; the simulation 10). Consequently, the set of best values parameters for the DTM model is:  $ice_{thr}$  is 5%,  $coast_{thr}$  is 150 km and  $ice_{time}$  is 45 days. However, our results are not very sensitive to the values tested in those experiments.

## 2.2. Inputs of the driftwood transport model

The DTM model needs three climatic fields as inputs: sea ice velocity, sea ice concentration and the ocean surface currents. These inputs are derived here from the results of the ocean-ice model NEMO-LIM (version 3.5; Barthélemy et al., 2015). OPA, the oceanic component of NEMO-LIM, is a finite difference, hydrostatic, primitive equation model (Madec, 2008). LIM, the sea ice component, uses an elastic-viscous-plastic (EVP) rheology (Hunke and Dukowicz, 1997) on a C-grid (Bouillon et al., 2009), an ice thickness distribution and a multi-layer halo-thermodynamic module (Vancoppenolle et al., 2009). The spatial resolution of NEMO-LIM is  $1^\circ$  on the global tripolar ORCA1 grid. The atmospheric forcing used in NEMO-LIM simulations is based on NCEP/NCAR reanalyses (Kalnay et al., 1996).

Additionally, Global Climate Models (GCMs) in the framework from the third phase of the Palaeoclimate Modelling Intercomparison Project (PMIP3; Otto-Bliesner et al., 2009), for which the interest variables, are available are used to drive DTM model during the Mid-Holocene. While the NEMO-LIM simulation is driven by an atmospheric reanalysis, the GCMs include an interactive atmospheric component, meaning that any bias in their wind field, for instance, may have a significant impact of the driftwood trajectories. Sea ice velocity is not available for all GCMs (except HadGEM2-CC and HadGEM-ES) and is derived from sea ice transport. See Table 1 for the name and modelling centre corresponding to each GCM.

The International Arctic Buoy Programme (IABP) C buoy dataset (Rigor, 2015) for the period 1992–2011 is used to evaluate modelled sea ice velocity. The sea ice velocity derived from buoy positions covers the Arctic Ocean (excluding the East Greenland Current) and is provided on a 100-km resolution regular grid with a temporal resolution of 12 h. Over the entire period, only 6 days have missing

data. It is important to note that a very small number of buoys cover the region off the Siberian coasts. Consequently, the sea ice velocity evaluation for this region is very uncertain.

The mean sea ice drift pattern from observations over the 1992–2011 period (Fig. 1) captures the main features of the Arctic sea ice drift, i.e. BG and TPD (Gordienko, 1958; Colony and Thorndike, 1984). The pattern of sea ice velocity for NEMO-LIM is similar to observations except that the BG is not completely closed and velocities are particularly weak in North Greenland and Ellesmere Island. The NEMO-LIM slightly underestimates sea ice drift averaged over the whole Arctic (4.84 km/day against 5.30 km/day for IABP buoys over the 1992–2011 period) except for the East Greenland Current where the sea ice drift is too high (as in Massonnet et al., 2011). The patterns of GCM sea ice velocity are generally characterised by a strong BG and a weak TPD (except for the CNRM-CM5 model). The CNRM-CM5 and HadGEM2-ES models overestimate the sea ice drift compared to the buoy observations over the 1992–2004 period (7.36 km/day for CNRM-CM5, 7.01 km/day for HadGEM2-ES and 5.12 km/day for observation; output of the GCMs is only available up to 2004). MPI-ESM-P and HadGEM2-CC are closed to the mean observed drift (5.15 km/day and 4.55 km/day) while the CSIRO-Mk3-6-0 and GISS-E2-R underestimate the drift (3.87 km/day and 2.69 km/day).

The evaluation of sea ice concentration from all models is based on the global reprocessed dataset (OSI-409-a) from OSI SAF (EUMETSAT OSI SAF, 2015) over the same period as for sea ice velocity (1992–2011). The spatial resolution of OSI SAF sea ice concentration dataset is 10 km. Based on daily data, we analyse only here the summer (JAS) mean sea ice concentration since the driftwood transport mainly depends on the summer sea ice concentration.

NEMO-LIM overestimates sea ice concentration, especially in the Beaufort Sea, Chukchi Sea and East Siberian Sea (the average summer sea ice extent obtained from NEMO-LIM is  $10.65 \cdot 10^6 \text{ km}^2$  against  $9.61 \cdot 10^6 \text{ km}^2$  for OSI SAF satellites data over the 1992–2011 period). The GCMs (except CSIRO-Mk3-6-0 for which the sea ice extent is overestimated –  $11.50 \cdot 10^6 \text{ km}^2$ ) underestimate the extent at Fram Strait and in the Atlantic Sector of the Arctic. The sea ice extent is  $7.49 \cdot 10^6 \text{ km}^2$ ,  $6.04 \cdot 10^6 \text{ km}^2$ ,  $8.33 \cdot 10^6 \text{ km}^2$ ,  $8.94 \cdot 10^6 \text{ km}^2$  and  $7.45 \cdot 10^6 \text{ km}^2$  for CNRM-CM5, GISS-E2-R, HadGEM-CC, HadGEM2-ES and MPI-ESM-P respectively against  $10.12 \cdot 10^6 \text{ km}^2$  from OSI SAF satellites over the 1992–2004 period. Even though the sea ice concentration is, for most of GCMs, too weak nearby the coast compared to the observations, the simulated Arctic sea ice concentration pattern is globally well represented.

## 3. Experimental design

### 3.1. Reference run for the present period

The first step is to obtain a reference state of the spatial

**Table 1**  
PMIP3/CMIP5 GCMs used in this study.

Model name	Modelling centre	Reference
CNRM5-CM5	Centre National de Recherches Meteorologiques Centre Europeen de Recherche et Formation Avancees en Calcul Scientifique	Voldoire et al. (2013)
CSIRO-Mk3L-1-2	Commonwealth Scientific and Industrial Research Organization in collaboration with Queensland Climate Change Centre of Excellence	Rotstayn et al. (2010)
GISS-E2-R	NASA Goddard Institute for Space Studies and Center for Climate Systems Research	Schmidt et al. (2014)
HadGEM2-CC	Met Office Hadley Centre	Collins et al. (2011)
HadGEM2-ES	Met Office Hadley Centre	Collins et al. (2011)
MPI-ESM-P	Max Planck Institute for Meteorology	Stevens et al. (2013)



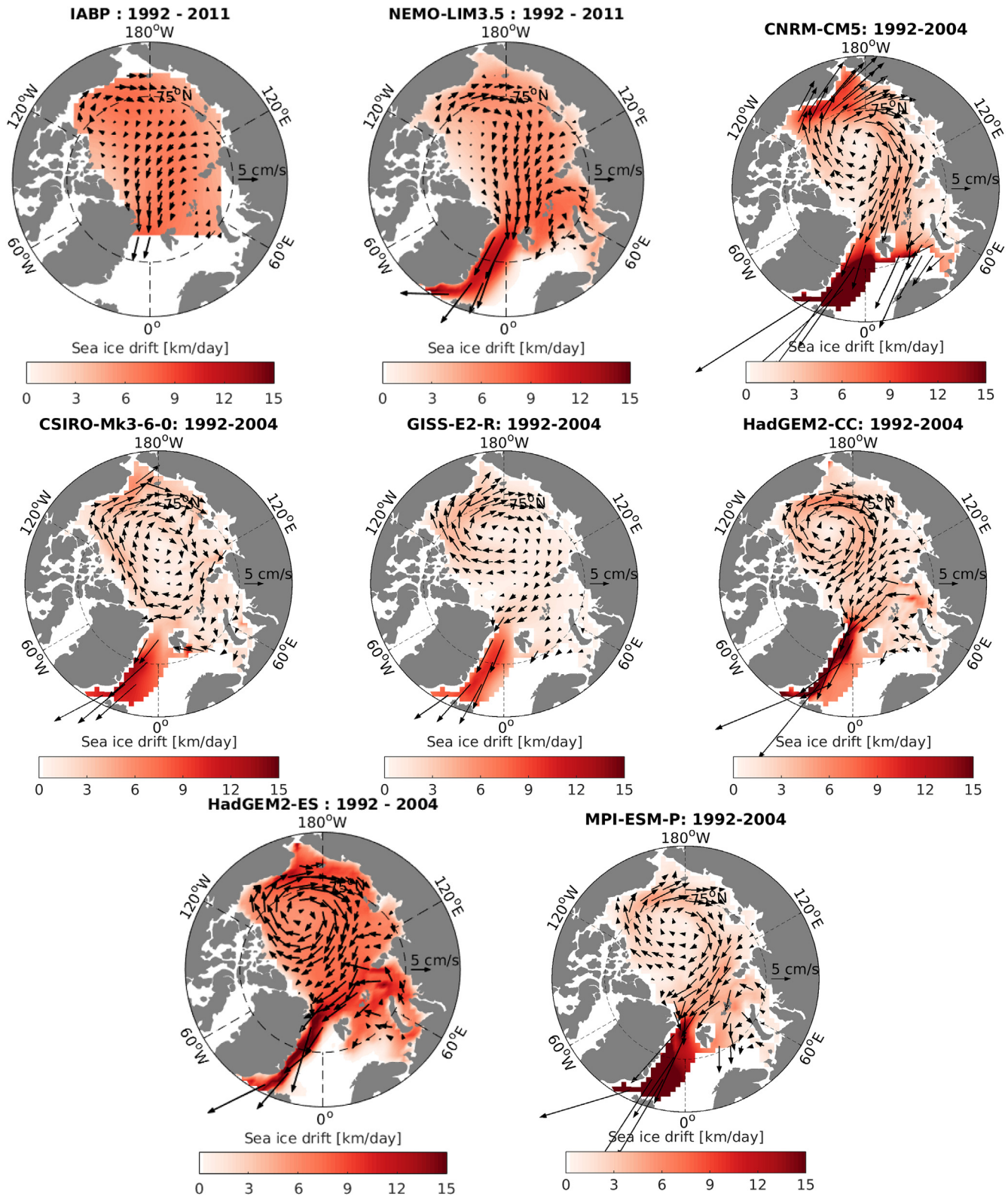


**Fig. 1.** Mean Arctic sea ice drift for IABP buoys (1992–2011), NEMO-LIM (1992–2011) and GCMs (1992–2004). For readability, the drift vectors are interpolated onto a common grid.

driftwood distribution simulated by the DTM model for the present period (1992–2011). The inputs of the DTM model (i.e. the sea ice velocity, concentration and the sea surface current velocity) are continuous over 10 years for NEMO-LIM and 6 years for the GCMs (because their outputs are only available until 2004) to catch the

interannual variability of the sea ice drift. The simulation duration in the DTM model is 30 years. Consequently, for example when the NEMO-LIM outputs are used, after 10 and 20 years of the DTM model run, woods are again subjected to the same environmental conditions as at the beginning of the simulation. Finally, since the

driftwood departure occurs in spring and summer period (Alix, 2005), the wood departure is uniformly distributed all along this period in 7 waves within which 500 woods are simulated for each wave. These experiments are hereafter referenced as REF. NEMO-LIM and REF. GCMs (one experiment for each GCM; Table 2).

We also drive the DTM model with observed ice velocity in order to test the impact of climate model biases. As the dataset of sea ice velocity derived from IABP buoys does not contain any observation south of Fram Strait (Fig. 1), it was completed by the NEMO-LIM sea ice velocity. The results of the study of Massonnet et al. (2011) concluded that NEMO-LIM overestimates the sea ice drift for the East Greenland Current. Consequently, the sea ice velocity of NEMO-LIM are reduced by 20% before merging then with IABP data to obtain a full spatial coverage. Moreover, the ocean current velocities and the sea ice concentration used for the REF. IABP run (Table 2) are those of NEMO-LIM.

### 3.2. Impact of atmospheric change on the driftwood distribution

The two main features of the Arctic sea ice drift pattern (i.e. BG and TPD) are a direct response of the atmospheric circulation (Rigor et al., 2002; Thorndike, 1984) and are thus strongly influenced by atmospheric variability (Rigor and Wallace, 2004; Goose and Holland, 2005; Funder et al., 2011). At the paleo-timescales, the sea ice circulation is also influenced by the changing bathymetry or freshwater forcing (Prange and Lohmann, 2003). In the North Atlantic, the dominant mode of atmospheric variability is the North Atlantic Oscillation (NAO), which is associated with changes in the position and intensity of the Westerlies (Hurrell et al., 2003). The NAO has a clear impact in the Arctic (Rigor et al., 2002). When the NAO index (defined as the difference in normalised pressure between the Azores and Iceland) is negative, a large anticyclone centered in the Beaufort Sea induces a strong BG and a weak TPD (Kwok, 2000). Conversely, when the NAO index is highly positive, the BG is less developed and weaker (Rigor et al., 2002) because of a weaker anticyclone over the Beaufort Sea (Kwok, 2000). Additionally, for positive NAO, the gyre center is closer to the coast, the TPD is stronger and travels eastward through the North Pole (Rigor et al., 2002). In some years, the position change of TPD is accompanied by a large cyclonic circulation centered north of the Kara Sea (Rigor et al., 2002). However, it is rare to observe a predominant cyclonic situation and the BG still persists (Rigor et al., 2002). Finally, the East Greenland Current is faster and closer to the coast in NAO + situations (Kwok, 2000).

Because of its impact on sea ice drift, the NAO variability has also likely an influence on driftwood trajectories. This hypothesis has been used for instance to interpret past changes in driftwood deposit (Bennike, 2004; Funder et al., 2011; Klein et al., 2014; Hole and Macias-Fauria, 2017). We will test here if this influence of the NAO

can be illustrated using the driftwood model and is compatible with the common interpretation based on qualitative arguments. To do that, we drive the DTM model with the outputs of NEMO-LIM for two extreme years in terms of NAO index: 1995 (NAO index: 1.03) and 2010 (NAO index: −1.90). The configurations of the DTM model are the same as previously except that the model runs for environmental conditions of a particular year. In other words, for the NAO + run, the run is based on the sea ice velocity, concentration and ocean surface currents of 2010 during the whole simulation.

Since the sea ice models show some biases in sea ice velocity, we will also drive the DTM model with the sea ice velocity from NEMO-LIM model corrected using the IABP buoys, to be sure that these biases do not affect the main conclusions of our experiments. The velocity is corrected in the following way:

$$\mathbf{u}_{\text{CORRECTED MODEL}}(x, y, t) = \mathbf{u}_{\text{MODEL}}(x, y, t) - \bar{\mathbf{u}}_{\text{BIAS}}(x, y, t') \quad (3)$$

where  $\mathbf{u}_{\text{CORRECTED MODEL}}$  is the sea ice velocity from NEMO-LIM model corrected using IABP buoys,  $\mathbf{u}_{\text{MODEL}}$  is the sea ice velocity for NEMO-LIM model and  $\bar{\mathbf{u}}_{\text{BIAS}}$  is the mean difference in sea ice velocity between the model and observations over the whole period considered ( $\mathbf{u}_{\text{MODEL}}(x, y, t) - \mathbf{u}_{\text{IABP}}(x, y, t)$ ) for each month.

### 3.3. Application of driftwood transport model to Mid-Holocene

The second application is devoted to the Mid-Holocene (MH) period (6 ka BP), using the outputs of 6 GCMs (CNRM-CM5, CSIRO-Mk3-6-0, GISS-E2-R, HadGEM2-CC, HadGEM2-ES and MPI-ESM-P). The comparison with results of the DTM model for present-day conditions allows evaluating the potential impact of past changes in sea ice concentration and velocity on driftwood trajectories and thus a direct comparison with observed beaching. The Mid-Holocene period is well documented by model results since it is a standard experiment for PMIP but also by the abundant proxy data. The Mid-Holocene period is thus a classic period for past studies (Braconnot et al., 2007). At 6 ka BP, the Arctic sea ice extent was reduced compared to pre-industrial conditions (Fig. 2) due to a higher summer insolation at high latitudes at this time (Berger and Loutre, 1991). Some models present a large difference in summer sea ice concentration between both periods (HadGEM2-ES, CNRM-CM5 and HadGEM2-CC), while others present a weak decrease as CSIRO-Mk3-6-0 and MPI-ESM-P and even an increase for GISS-E2-R (Fig. 2). In the HadGEM2-ES model, the decrease in sea ice extent reaches  $2 \cdot 10^6 \text{ km}^2$  in summer, which is in the upper range of the values obtained in PMIP simulations (Goosse et al., 2013). By contrast, the mean pattern of sea ice drift for each GCM at 6 ka BP (Fig. A5) is very similar to that of the present period (Fig. 1).

The configuration of the DTM model is the same as in the two precedent applications. In order to identify the contribution of sea

**Table 2**

Characteristics of the model experiments, with the name of experiments (column 1), the input fields (columns 2–4), and the periods over which the experiments are carried out (columns 5–6). \*IABP buoys used in this study does not contain observations south of Fram Strait (Fig. 1), thus this dataset was completed by the sea ice velocity of NEMO-LIM reduced by 20% to be consistent with the observations (Massonnet et al., 2011).

SIM NAME	Inputs field			Period	
	ICE VEL	ICE CONC	OCEAN CURRENTS	VEL	CONC
REF. IABP	IABP–NEMO-LIM*	NEMO-LIM	NEMO-LIM	1992–2011	1992–2011
REF. NEMO-LIM	NEMO-LIM	NEMO-LIM	NEMO-LIM	1992–2011	1992–2011
REF. GCMs	GCMs	GCMs	GCMs	1992–2011	1992–2011
EXP. NAO+	NEMO-LIM	NEMO-LIM	NEMO-LIM	1995	1995
EXP. NAO-	NEMO-LIM	NEMO-LIM	NEMO-LIM	2010	2010
EXP. MH1	GCMs	GCMs	GCMs	6 ka BP	1992–2011
EXP. MH2	GCMs	GCMs	GCMs	1992–2011	6 ka BP
EXP. MH3	GCMs	GCMs	GCMs	6 ka BP	6 ka BP

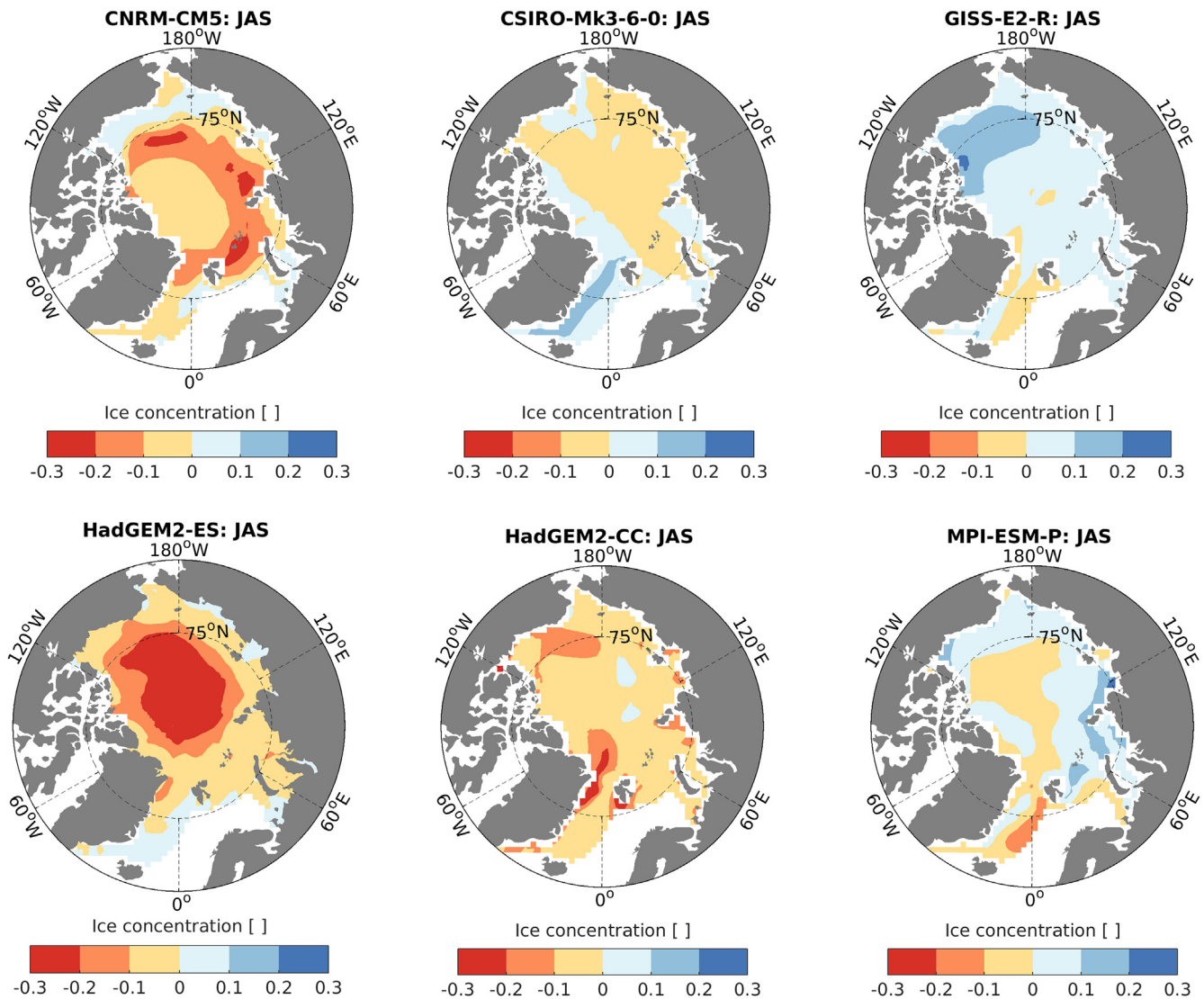


**Fig. 2.** Difference between Arctic summer (JAS) sea ice concentration over the MidHolocene period and present period (1992–2004) for all GCMs.

ice extent and velocity changes at 6 ka BP, three experiments for 6 ka BP (MH1, MH2 and MH3 experiments) are compared to the standard experiment (REF experiment). The characteristics of each experiment are presented in Table 2. The characteristics (MH1) uses the present day sea ice concentration but the sea ice velocity from the Mid-Holocene period. The second experiment (MH2) uses the present day sea ice velocity but sea ice concentration from the Mid-Holocene period. This way, we can assess whether a more restrained sea ice extent plays a role in the driftwood distribution. The last experiment (MH3) uses sea ice concentration and sea ice velocity from the Mid-Holocene period.

#### 4. Results and discussion

##### 4.1. Driftwood transport model evaluation over 1992–2011

Fig. 3 shows some representative examples of driftwood trajectories and the average of Canadian and Siberian driftwood distributions for the present period (1992–2011) derived from the simulations of the DTM model using the sea ice velocity derived from observations (REF. IABP) and the NEMO-LIM model outputs (REF. NEMO-LIM).

First of all, as in the driftwood observations (Hellmann et al., 2017; Hole and Macias-Fauria, 2017), wood beaching mainly occurs in the Arctic Ocean in REF. IABP (i.e. in North Greenland, Ellesmere Island and Svalbard; Fig. 3). Indeed, less than 5% of all modelled driftwood (Canadian and Siberian woods) ends up south of Fram Strait. North Greenland and Ellesmere Island are the main arrival regions for the Canadian driftwood in REF. IABP, in agreement with the results of Hellmann et al. (2017). Therefore, the Canadian woods end up in a restricted geographical region. For Siberian woods, the fraction of driftwood passing Fram Strait is higher than for the Canadian driftwood (Fig. 3; 1% for the Canadian against 8% for the Siberian) because of the Siberian woods are rapidly taken into the TPD and go further south compared to Canadian wood. Moreover, the proportion of Siberian driftwood arriving in Svalbard is larger compared to the Canadian, as in observations (Hellmann et al., 2017). The driftwood proportion ending up to the south of Fram Strait in REF. NEMO-LIM experiment is larger (24.8%) than the REF. IABP experiment meaning that NEMO-LIM tends to overestimate the proportion of driftwood in southern regions. On average over all the DTM REF experiments using the GCMs outputs, the Siberian driftwood simulated is consistent with the REF. IABP since the most of driftwood mainly



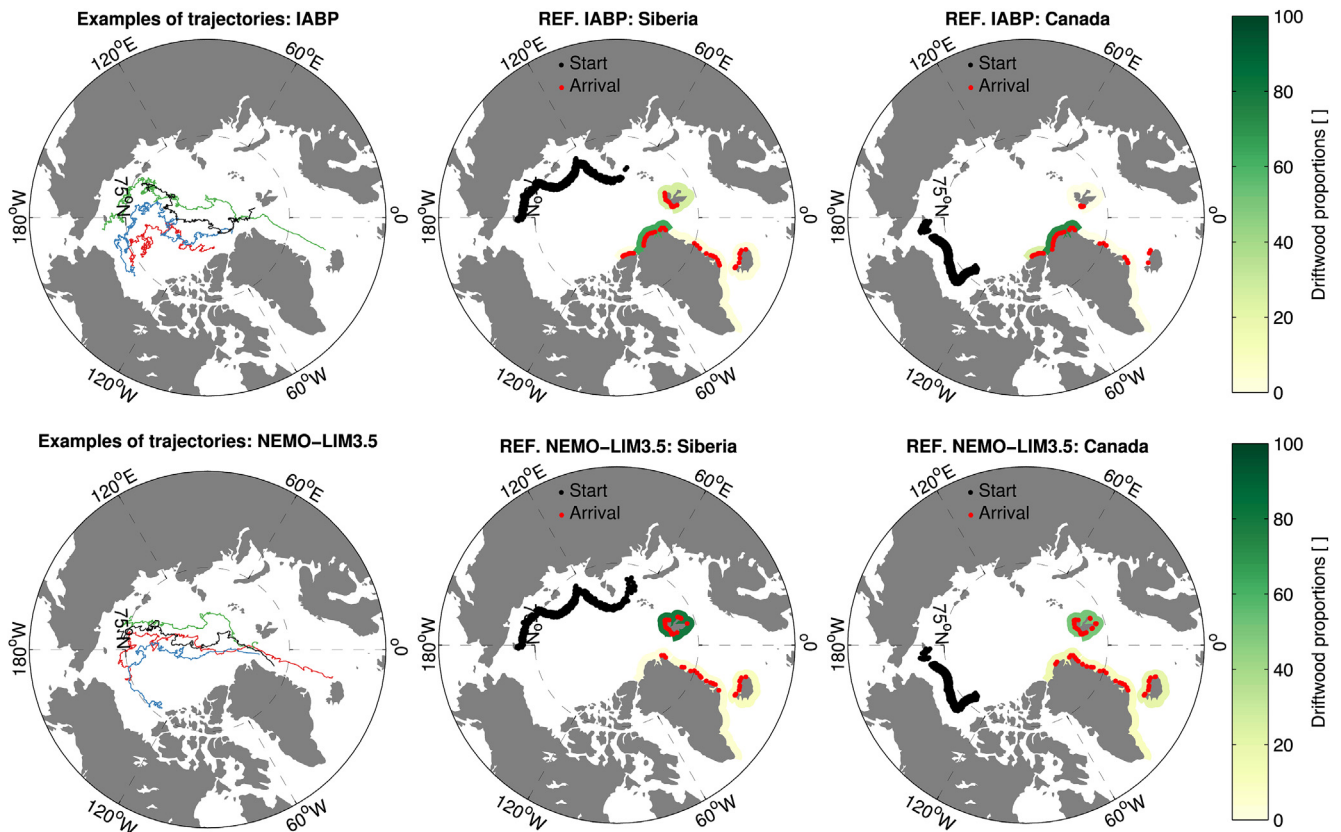


**Fig. 3.** Examples of driftwood and fractions of driftwood originating from either Siberia or Canada that is deposited at each location relative to all beached driftwood. These results come from the DTM simulations using the IABP buoys and NEMO-LIM outputs. In black, the initial positions of driftwood and in red, the final positions after the travel. (For interpretation of the references to colour in this figure legend, the reader is referred to the Web version of this article.)

ends up in North Greenland (46%) and Svalbard (24%). As much for the Canadian driftwood, the GCMs experiments show an overestimation of the driftwood export to the Atlantic (24% for the Canadian and 29% for the Siberian driftwood beach in South Greenland or Iceland on average). However, the main arrival coast for the Canadian driftwood derived from the experiments using the GCMs outputs is North Greenland (53%) as the REF. IABP.

Those driftwood trajectories are consistent with sea ice drift simulated in the models with a clear difference between the simulations using the NEMO-LIM models and GCMs for the present period (Fig. 1). For the GCMs, the BG is often very strong, leading woods to be often trapped into the BG before being released. It is the opposite for NEMO-LIM where the TPD is wider resulting in more direct trajectories towards Fram Strait (Fig. 3). The REF. NEMO-LIM experiment shows that most of Siberian driftwood (80%) ends up in Svalbard while Canadian driftwood ends up on the Arctic coasts in a slightly more homogeneous way (Fig. 3). Wood (Canadian and Siberian) preferentially ends up in Svalbard (50%) and no wood beached in Ellesmere Island in contrast to observation (Fig. 3; England et al., 2007). For the GCMs presenting a wide BG and a weak TPD as the CSIRO-Mk3-6-0, HadGEM2-CC and HadGEM-ES GCMs, a small fraction is exported to Fram Strait leading to a beaching in North Greenland (Fig. 6). In the opposite situation (weaker BG and stronger TPD) as for the CNRM-CM5 GCM, Canadian wood mainly ends up to the south of Fram Strait and Svalbard while the Siberian wood is mainly deposited in Svalbard. In the other GCMs (GISS-E2-R and MPI-ESM-P), the driftwood distribution is more distributed over the whole Arctic coasts (Fig. 6). Unfortunately, the REF experiment using the GISS-E2-R outputs simulates no Canadian driftwood deposit due to the too

weak sea ice concentration near the Canadian coasts.

#### 4.2. Impact of atmospheric change on the driftwood distribution

The patterns of sea ice drift for two specific years derived from NEMO-LIM are in agreement with the expected response to NAO (Kwok, 2000; Funder et al., 2011; Rigor et al., 2002). We observe a weak BG and a strong TPD in 1995 (NAO + situation) and the opposite case in 2010 (NAO- situation; Figs. 4 and A6). The NAO has nearly no impact on the distribution of Siberian driftwood (Fig. A6). The effect is larger for Canadian driftwood. In 2010, the strong BG drives the Canadian driftwood closer to the Ellesmere Island and North Greenland (Fig. 4). At the opposite, in 1995 when the BG is weaker, the Canadian driftwood tends to rapidly reach the TPD making beaching in Ellesmere Island or North Greenland almost impossible (Fig. 4). In 2010, 18% of driftwood ends up in North Greenland, while 7% does in 1995 (Fig. 5). We also observe that the arrival positions of driftwood in North Greenland is further west in 2010 than 1995 (Fig. 4). Because of the strong TPD in NAO + conditions, a large part of Canadian driftwood ends up to the south of Fram Strait. Indeed, the Canadian driftwood proportion ending up in Iceland and South Greenland in 1995 is 69% against 16% in 2010 (Fig. 5). Finally, the proportion increase of Canadian driftwood in Svalbard in NAO- situation is due to a strong BG bringing driftwood to the Siberian coasts and thus increasing the probability of beaching in Svalbard (Figs. 4 and 5).

Because of biases in NEMO-LIM sea ice velocity north of Ellesmere Island, very few woods end up in Ellesmere Island. Thanks to the correction of NEMO-LIM sea ice velocity on the basis of IABP buoys, the sea ice velocity for this region is more directed to the

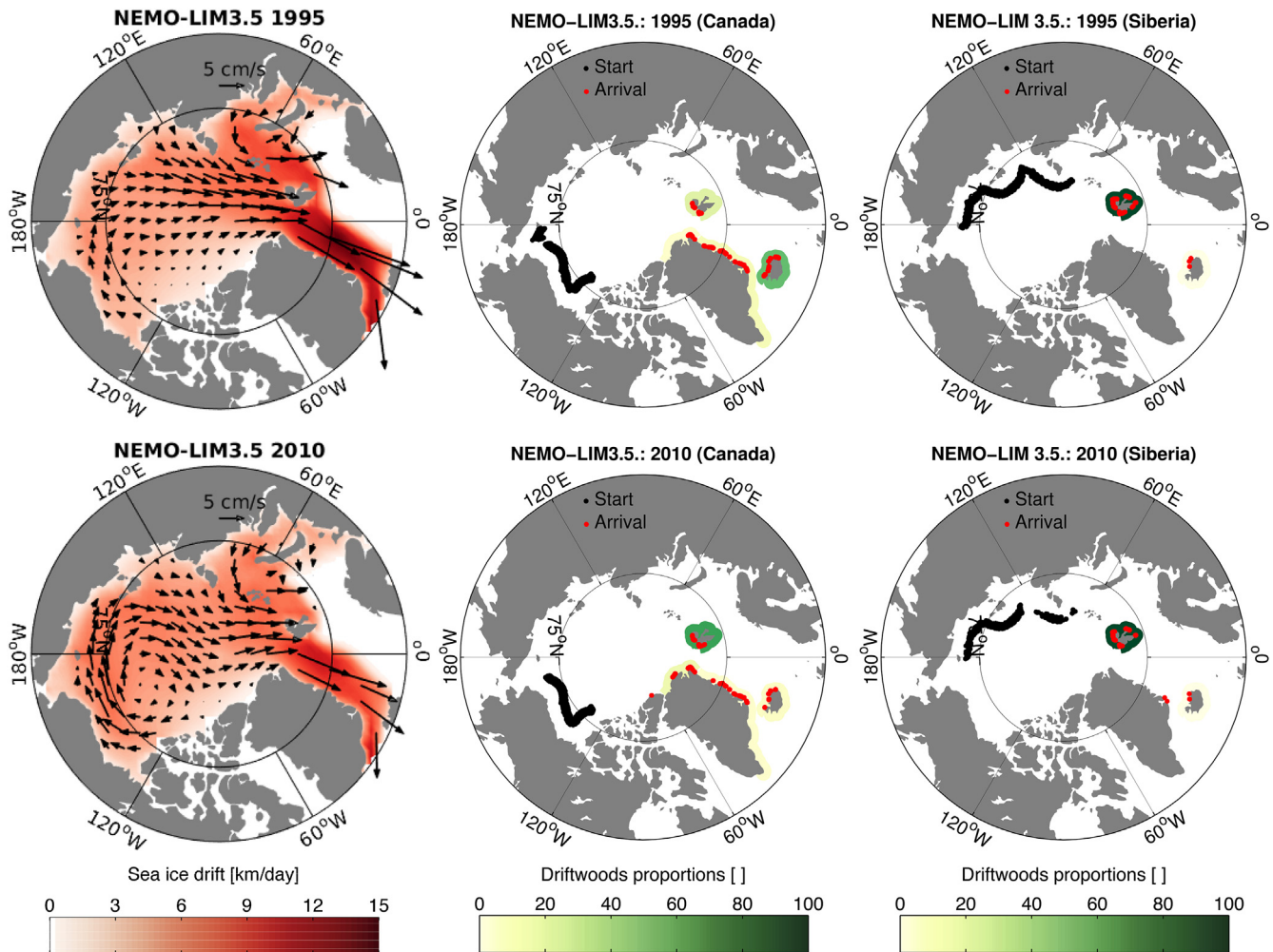


**Fig. 4.** (A and d) Mean annual patterns of sea ice drift of NEMO-LIM for 1995 (NAO index is 1.05) and 2010 (NAO index is -1.90). (b, c, e and f) Fractions of driftwood originating from either Siberia or Canada that is deposited at each location relative to all beached driftwood. These results come from the two simulations of driftwood model using NEMO-LIM for repeated conditions 1995 and these of 2010. In black, the initial positions of driftwood and in red, the final positions after the travel. (For interpretation of the references to colour in this figure legend, the reader is referred to the Web version of this article.)

land (Fig. 4 and A6). Generally, a small change in the sea ice drift pattern (here, due to the sea ice velocity correction) has a large impact on the spatial driftwood distribution. Indeed, after correction, no driftwood (Siberian or Canadian) passes Fram Strait in NAO- situation (Figs. 4 and 5). Even though the Canadian driftwood distribution is relatively similar between both NAO situations (Fig. 5), we observe that driftwood in 1995 ends up further east in North Greenland than in 2010 (Fig. A6). In NAO + conditions, for the Siberian driftwood, driftwood is more evenly distributed on the whole Arctic coasts than for non-corrected NEMO-LIM due to a small change in the direction of TPD (Fig. 5). The large part of Siberian driftwood beaching in North Greenland in 2010 (77%; Fig. 5) is explained by the strong BG and a shift in TPD (unlike non-corrected sea ice velocity), leading to a driftwood deposit in Ellesmere Island and North Greenland (Fig. A6).

#### 4.3. Application of driftwood transport model to Mid-Holocene

On the basis of a large driftwood data base, Hole and Macias-Fauria (2017) suggested a shift towards more positive NAO conditions during the Mid-Holocene associated with a reduced BG, combined with an expansion of the TPD. Compared to the present period, the TPD would have been slightly shifted to the west.

Consequently, the driftwood deposit was higher in North Greenland in comparison to the present period (Hole and Macias-Fauria, 2017).

Our experiments with the DTM model driven by the GCM outputs during the Mid-Holocene (MH3 experiment, Table 2) generally agree with the observed changes in deposit (Fig. 6). In particular, the MH3 experiment, using all the GCM outputs except CNRM-CM5 and GISS-E2-R, shows an increase of driftwood beaching in North Greenland at 6 ka BP in comparison to the present period (REF experiment; Fig. 6). This change in driftwood deposit is explained by a reduced BG and a westward shift of the TPD. These results match well with the driftwood records (Bennike and Weidick, 2001; Nixon et al., 2016; Dyke et al., 1997; Hole and Macias-Fauria, 2017). Hole and Macias-Fauria (2017) suggested that the changes in driftwood deposit may be due to relatively large changes in the sea ice circulation. However, in these GCMs, the change in sea ice circulation between both periods is small (Figs. 1 and A.5). Consequently, small local changes in sea ice circulation are enough to explain large changes in driftwood landing.

In contrast, the driftwood proportion in North Greenland for the MH3 experiment driven by CNRM-CM5 outputs is weaker than for the present period (REF experiment). The Canadian driftwood proportion is higher for South Greenland and weaker for Svalbard



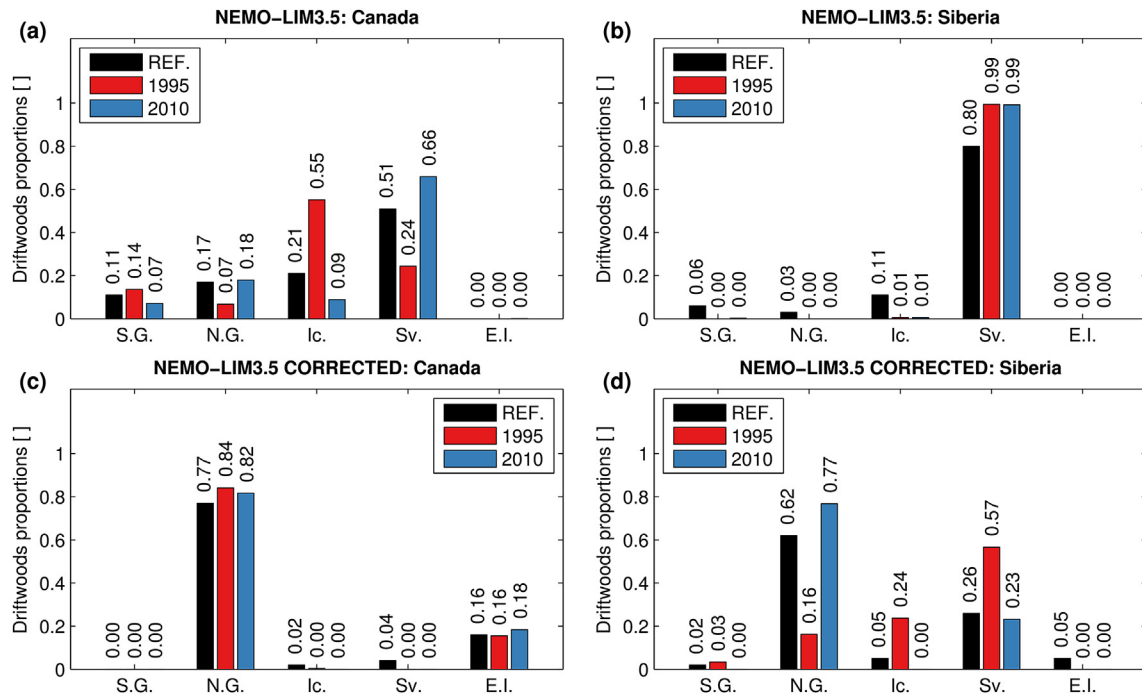


**Fig. 5.** Average proportions of driftwood for arriving in selected regions of the Arctic (S.G.: South Greenland; N.G.: North Greenland; Ic.: Iceland; Sv.: Svalbard; E.I.: Ellesmere Island) relative to all beached driftwood departing from Siberian and Canadian coasts. These results coming from the two simulations of driftwood transport model using NEMO-LIM (a–b) and corrected NEMO-LIM (c–d) for repeated conditions 1995 and these of 2010.

compared to the present period (Fig. 6). This result can be explained by a too weak westward shift of the TPD. Consequently, driftwood comes closer to North Greenland but not enough to observe a beaching in this region. However, this shift in TPD induces a reduction of the proportion of Canadian driftwood in Svalbard in the MH3 experiment compared to the REF experiment. The Siberian driftwood proportion beaching in Svalbard is also larger at 6 ka BP than now, supporting a stronger TPD.

The driftwood studies mainly mentioned a change in sea ice circulation to explain a past change in driftwood deposit for the mid-Holocene (e.g. Hellmann et al., 2013; Hole and Macias-Fauria, 2017) but in our experiments, the impact of sea ice extent change is also present. Consequently, the driftwood deposit change cannot be only interpreted as a change in sea ice dynamic even though this change has a larger impact than that of the change in sea ice extent. By comparing the MH1 (sea ice velocity during the Mid-Holocene and sea ice concentration at present period) and MH3 (full Mid-Holocene conditions) experiments, we notice large differences in driftwood landing (Fig. 6). Due to the weak sea ice concentration at Fram Strait during the Mid-Holocene (Fig. 2), wood tends to sink faster than during the present period. Additionally, Canadian woods taken in the BG tend to sink because of the reduced ice cover at 6 ka BP. For example, the Canadian wood in the MH3 CNRM-CM5 experiment at Fram Strait sinks before reaching South Greenland or Iceland. This leads to a relative increase in driftwood deposit in Svalbard and a decrease in South Greenland in MH3 experiment compared to MH1 experiment (Fig. 6). The impact of the sea ice concentration change is also present in the MH3 HadGEM2-CC experiment. The Canadian driftwood does not have the time to reach the Ellesmere Island once driftwood has reached North Greenland because of weak sea ice concentration around Fram Strait. Therefore, driftwood sinks before reaching Ellesmere Island, leading to a relative increase of driftwood landing in North Greenland and a decrease in Ellesmere Island.

The experiments driven by the HadGEM2-ES outputs show an

interesting synergy between changes in sea ice velocity and extent not present in the other GCMs. Using sea ice concentration during the Mid-Holocene and sea ice velocity for the present period in the DTM model (MH2 experiment), we do not see a large difference with the REF experiment. However, the results of REF and MH1 experiments are different. For Canadian wood, compared to the present period, the proportion of driftwood deposit is higher in Ellesmere Island and weaker in North Greenland (Fig. 6). This change can be explained by a slight westward shift in TPD. Additionally, the difference results of REF and MH3 HadGEM2-ES is far more large than that of REF and MH1 experiments. For the Canadian wood, no driftwood ends up on a coast during all the MH3 experiment. This result illustrates that the impact of the combination of the two changes (sea ice extent and circulation) is not equivalent to the sum of the individual contributions. The response is non-linear and the changes of sea ice concentration combined with the ones in velocity have thus a decisive impact on the driftwood transport during the Mid-Holocene. In HadGEM2-ES model, the BG is slightly stronger at 6 ka BP leading to a transport of Canadian wood closer to the Siberian coasts where the sea ice concentration is very low. Consequently, wood rapidly sinks after their departure from the Canadian coasts. We have tested the sensitivity of this conclusion using values of  $ice_{time}$  up to 180 days without a significant impact on our results showing they are independent of the parameter choice. The total absence of Canadian driftwood deposit in MH3 experiment with the HadGEM2-ES outputs is in clear disagreement with observations (Hole and Macias-Fauria, 2017). The unrealistic behaviour of Canadian driftwood is probably related to an underestimation of the ice extent for 6 ka BP, HadGEM2-ES being one of the model with the largest decrease in summer ice extent among PMIP3 models (Goosse et al., 2013).

## 5. Conclusions

Proxy system models have proved their utility for many

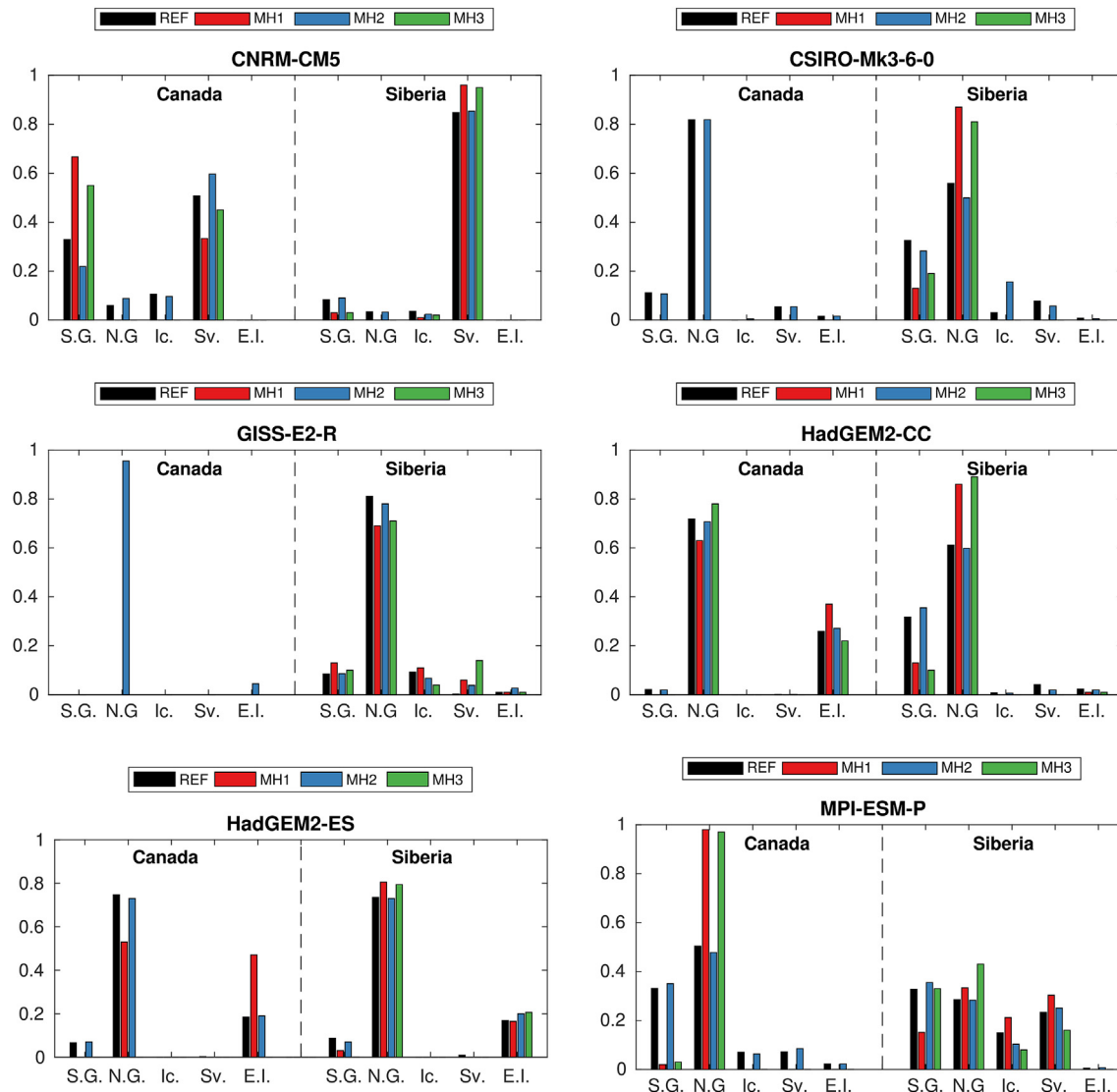


**Fig. 6.** Proportions of driftwood for each arrival coast (S.G.: South Greenland; N.G.: North Greenland; Ic.: Iceland; Sv.: Svalbard; E.I.: Ellesmere Island) relative to all beached driftwood and according to the depart zone (Siberian or Canadian coasts). These results come from the four experiments (REF, GCM, MH1, MH2 and MH3; see Table 2 for details) with the driftwood transport model using the GCMs outputs.

paleoclimate observations. Our study demonstrates that a relatively simple model is able to reproduce the main characteristics of observed driftwood. It is thus an interesting tool to interpret past changes and to evaluate climate model results. The comparison between simulated results and observations performed here is not quantitative because of the uncertainties in the wood age and the driftwood origin collected on the shore. Nevertheless, driven by the output of climate models, the DTM model simulates the main factors controlling driftwood trajectories and their potentially non-linear interactions in order to simulate the variable that is observed (i.e. driftwood deposit). Thanks to our model, we are able to bridge the gap between the paleoclimate observations and climate models (e.g. GCMs) by bringing climate model outputs into the proxy space. The qualitative comparison between model results and observations is thus much more direct and objective and this constitutes an important step towards a more objective quantification of the differences between climate model results and observations.

Many studies interpret past changes in driftwood deposit as modifications of the atmospheric circulation, in particular as a shift

in NAO. Consequently, to directly study the impact of an atmospheric circulation change on the spatial distribution of driftwood, we performed two simulations with the DTM model driven by the outputs of NEMO-LIM sea ice model for two widely different NAO conditions. The results exhibit a clear dependence of the spatial driftwood distribution on the atmospheric circulation. Indeed, in NAO- situation, when the BG is strong and the TPD weak, the driftwood ends up north of Fram Strait, mainly in Ellesmere and North of Greenland. In contrast, the NAO + conditions are characterised by a weak BG and a strong TPD leading to a larger driftwood deposit south of Fram Strait (South Greenland and Iceland).

A second application is devoted to the Mid-Holocene period (at 6 ka BP) using the DTM model driven by the outputs of six GCMs. Compared to the present period, a decrease in the summer sea ice extent during the Mid-Holocene is observed due to orbital forcing. We have shown that most of DTM simulations driven the GCMs outputs are in agreement with the driftwood records at 6 ka BP. The driftwood deposit change during the Mid-Holocene compared to the present period is mainly explained by a change in the sea ice circulation. Compared to the present period, we deduced a reduced

BG and a westward shift of the TPD from our experiments at 6 ka BP. Specifically, our experiments have shown that small local changes in sea ice circulation suffice to explain the observed change in driftwood deposit at 6 ka BP compared to the present period. Therefore, large changes in driftwood deposit should not necessarily be interpreted as large changes in sea ice velocity and atmospheric circulation. The interpretation of driftwood in term of significant local circulation changes and their links with large scale patterns must thus be performed with caution. Additionally, a change in sea ice circulation associated with a change in sea ice extent may have a much larger impact on driftwood deposit than the sum of two individual impacts. For instance, in contrast to the present period, no Canadian driftwood ends up on Ellesmere Island and North Greenland during the Mid-Holocene in the DTM model driven by HadGEM2-ES. Taking into account this non linear behaviour is critical to interpret the observations and also to evaluate climate models using driftwood data. In this context, the use of a model that explicitly simulates driftwood trajectory provides thus as a relevant tool to interpret driftwood deposit.

### Authors contributions

HG and QD designed the experiments. QD, OL and DD collected the observation databases. QD developed the model, performed the simulations and produced the figures. QD and HG developed the diagnostics, analysed the results. QD prepared the manuscript with contributions from HG, OL and DD.

### Data availability

The source code of the DTM model is available on public repository (<https://github.com/dalaiden/DTM-model>). The DTM outputs used in this study are available upon request. All GCMs results used to drive the DTM model in this study are publicly available and can be obtained from World Climate Research Programme (<https://esgf-node.lnl.gov>). The NEMO-LIM outputs used in this study are available upon request.

### Conflicts of interest

The authors declare that they have no conflict of interest.

### Acknowledgements

We would like to thank J. Jungclaus, H. Helmuth and G. Schmidt for their help to infer the sea ice velocity from sea ice transport. We acknowledge the World Climate Research Programme Working Group on Coupled Modelling, which is responsible for CMIP, and we thank the climate modelling groups (listed in Table 1 of this paper) for producing and making available their model outputs. We sincerely thank the editor and two reviewers for their constructive remarks which helped to improve the manuscript. HG is Research Director at F.R.S.-FNRS, Belgium; DD is funded by the EU Horizon 2020 PRIMAVERA project, grant agreement no. 641727.

### Appendix A. Supplementary data

Supplementary data related to this article can be found at <https://doi.org/10.1016/j.quascirev.2018.05.004>.

### References

Alix, C., 2005. Deciphering the impact of change on the driftwood cycle: contribution to the study of human use of wood in the Arctic. *Glob. Planet. Change* 47, 83–98. <https://doi.org/10.1016/j.gloplacha.2004.10.004>.

- Barthélemy, A., Fichet, T., Goosse, H., Madec, G., 2015. Modeling the interplay between sea ice formation and the oceanic mixed layer: limitations of simple brine rejection parameterizations. *Ocean. Model.* 86, 141–152.
- Bennike, O., 2004. Holocene sea-ice variations in Greenland: onshore evidence. *Holocene* 14 (4), 607–613. <https://doi.org/10.1191/0959683604h1722rr>.
- Bennike, O., Weidick, A., 2001. Late quaternary history around nioghalvfjærdssjøen and jøkelbugten, north-east Greenland. *Boreas* 30 (3), 205–227. <https://doi.org/10.1111/j.1502-3885.2001.tb01223.x>.
- Berger, A., Loutre, M., 1991. Insolation values for the last 1000000 years. *Quat. Sci. Rev.* 10, 297–317.
- Bouillon, S., Morales Maqueda, M.A., Legat, V., Fichet, T., 2009. An elastic-viscous-plastic sea ice model formulated on Arakawa B and C grids. *Ocean. Model.* 27 (3–4), 174–184. <https://doi.org/10.1016/j.ocemod.2009.01.004>.
- Braconnot, P., Otto-Bliesner, B., Harrison, S., Joussaume, S., Peterchmitt, J.-Y., Abe-Ouchi, A., Crucifix, M., Driesschaert, E., Fichet, T., Hewitt, C.D., Gageyama, M., Kitoh, A., Laîné, A., Loutre, M.-F., Marti, O., Merkel, U., Ramstein, G., Valdes, P., Weber, S.L., Yu, Y., Zhao, Y., 2007. Results of PMIP2 coupled simulations of the Mid-Holocene and Last Glacial Maximum –; Part 1: experiments and large-scale features. *Clim. Past* 3 (2), 261–277. <https://doi.org/10.5194/cp-3-261-2007>.
- Collins, W.J., Bellouin, N., Doutriaux-Boucher, M., Gedney, N., Halloran, P., Hinton, T., Hughes, J., Jones, C.D., Joshi, M., Liddicoat, S., Martin, G., O'Connor, F., Rae, J., Senior, C., Sitch, S., Totterdell, I., Wiltshire, A., Woodward, S., 2011. Development and evaluation of an earth-system model – HadGEM2. *Geosci. Model Dev.* 4, 1051–1075. <https://doi.org/10.5194/gmdd-4-997-2011>.
- Colony, R., Thorndike, A., 1984. An estimate of the mean field of Arctic sea ice motion. *J. Geophys. Res.* 89 (C6), 10623–10629. <https://doi.org/10.1029/JC089iC06p10623>.
- Dee, S., Emile-Geay, J., Evans, M., Allam, A., Steig, E., Thompson, D., 2015. PRYSM: an open-source framework for ProX System Modeling, with applications to oxygen-isotope systems. *J. Adv. Model. Earth Syst.* 7, 1220–1247. <https://doi.org/10.1002/2015MS000447>.
- Dyke, A., England, J., Reimnitz, E., Jette, H., 1997. Changes in driftwood delivery to the Canadian arctic archipelago. *Arct. Anthropol.* 50 (1), 1–16.
- Eggertsson, O., 1993. Origin of the driftwood on the coasts of Iceland; a dendro-chronological study. *Jökull* 43, 15–32.
- Eggertsson, O., 1994. Driftwood as an indicator of relative change in the influx of Arctic and Atlantic water into the coastal areas of Svalbard. *Polar Res.* 13 (2), 209–218.
- England, J., Lakeman, T., Lemmen, D., Bednarski, J., Stewart, T., Evans, J., 2007. A millennial-scale record of Arctic Ocean sea ice variability and the demise of the Ellesmere Island ice shelves. *Geophys. Res. Lett.* 35, 1–5.
- EUMETSAT OSI SAF, 2015. Global sea ice concentration reprocessing dataset 1978–2015 (v1.2). <http://www.osi-saf.org/>.
- Evans, M., Tolwinski-Ward, S., Thompson, D., Anchukaitis, K., 2013. Applications of proxy system modeling in high resolution paleoclimatology. *Quat. Sci. Rev.* 76, 16–28.
- Funder, S., Goosse, H., Jepsen, H., Kaas, E., Kjaer, K., Korsgaard, N., Larsen, N., Linderson, H., Lysa, A., Möller, P., Olsen, J., Willerslev, E., 2011. A 10,000-year record of Arctic Ocean sea-ice variability – view from the beach. *Science* 333, 747–750.
- Goosse, H., Holland, M., 2005. Mechanisms of decadal arctic climate variability in the community climate system model, version 2 (CCSM2). *J. Clim.* 18, 3552–3570.
- Goosse, H., Roche, D., Mairesse, A., Berger, M., 2013. Modelling past sea ice changes. *Quat. Sci. Rev.* 79, 191–206.
- Gordienko, P., 1958. Arctic ice drift: arctic sea ice: proceedings of the conference. *Natl. Res. Counc.* 98, 210–220.
- Hellmann, L., Kiryanov, A., Büntgen, U., 2016. Effects of boreal timber rafting on the composition of arctic driftwood. *Forests* 7 (257), 1–9.
- Hellmann, L., Tegel, W., Eggertsson, O., Schweingruber, F.H., Blanchette, R., Kiryanov, A., Gärtner, H., Büntgen, U., 2013. Tracing the origin of Arctic driftwood. *J. Geophys. Res. Biogeosciences* 118, 1–9.
- Hellmann, L., Tegel, W., Geyer, W., Kiryanov, A., Nikolaev, A., Eggertsson, O., Altman, J., Reinig, F., Morganti, S., Wacker, L., Büntgen, U., 2017. Dendro-provenancing of arctic driftwood. *Quat. Sci. Rev.* 162, 1–11.
- Hellmann, L., Tegel, W., Kiryanov, A.V., Eggertsson, Ö., Esper, J., Agafonov, L., Nikolaev, A.N., Knorre, A.A., Myglan, V.S., Churakova, O., Schweingruber, F.H., Nievergelt, D., Verstege, A., Büntgen, U., 2015. Timber logging in central Siberia is the main source for recent Arctic driftwood. *Arct. Antarct. Alp. Res.* 47 (3), 449–460. <https://doi.org/10.1657/AAAR0014-063>.
- Hole, G.M., Macias-Fauria, M., 2017. Out of the woods: driftwood insights into Holocene pan-Arctic sea ice dynamics. *J. Geophys. Res. Oceans* 122 (9), 7612–7629. <https://doi.org/10.1002/2017JC013126>.
- Hunke, E.C., Dukowicz, J.K., 1997. An elastic–viscous–plastic model for sea ice dynamics. *J. Phys. Oceanogr.* 27 (9), 1849–1867. [https://doi.org/10.1175/1520-0485\(1997\)027<1849:AEVPMF>2.0.CO;2](https://doi.org/10.1175/1520-0485(1997)027<1849:AEVPMF>2.0.CO;2).
- Hurrell, J., Kushnir, Y., Visbeck, M., Ottersen, G., 2003. An overview of the North Atlantic oscillation. *The North Atlantic oscillation: climate significance and environmental impact*. In: *Geophysical Monograph Series*, vol.134, pp. 1–35.
- Häggblom, A., 1982. Driftwood in svalbard as an indicator of sea ice conditions. *Geografiska annaler. Ser. A, Phys. Geogr.* 64 (1/2), 81–94. <https://doi.org/10.2307/520496>.
- Kalnay, E., Kanamitsu, M., Kistler, R., Collins, W., Deaven, D., Gandin, L., Iredell, M., Saha, S., White, G., Woollen, J., Zhu, Y., Leetmaa, A., Reynolds, R., 1996. The NCEP/NCAR 40-year reanalysis project. *Bull. Am. Meteorological Soc.* 77 (3),



- 437–471. TNYRP;2.0.CO;2. [https://doi.org/10.1175/1520-0477\(1996\)077<0437:TNYRP>2.0.CO;2](https://doi.org/10.1175/1520-0477(1996)077<0437:TNYRP>2.0.CO;2).
- Kelly, M., Bennike, O., 1992. The quaternary geology of central North Greenland. *Rapp. Grøn. Geol. Unders.* pages 153, 34.
- Klein, F., Goosse, H., Mairesse, A., De Vernal, A., 2014. Model-data comparison and data assimilation of mid-Holocene Arctic sea ice concentration. *Clim. Past* 10 (3), 1145–1163. <https://doi.org/10.5194/cp-10-1145-2014>.
- Kwok, R., 2000. Recent changes in Arctic Ocean sea ice motion associated with the North Atlantic oscillation. *Geophys. Res. Lett.* 27 (6), 775–778.
- Madec, G., 2008. NEMO Ocean Engine. Technical Report. Institut Pierre-Simon Laplace (IPSL), Paris, France.
- Massonnet, F., Fichefet, T., Goosse, H., Vancoppenolle, M., Mathiot, P., König, C., 2011. On the influence of model physics on simulations of Arctic and Antarctic sea ice. *Cryosphere* 5, 687–699.
- Nixon, F.C., England, J.H., Lajeunesse, P., Hanson, M.A., 2016. An 11 000-year record of driftwood delivery to the western Queen Elizabeth Islands, Arctic Canada. *Boreas* 45 (3), 494–507.
- Otto-Bliesner, B.L., Joussaume, S., Braconnot, P., Harrison, S.P., Abe-Ouchi, A., 2009. Modeling and data syntheses of past climates: paleoclimate modelling Inter-comparison project phase II workshop. *Eos. Trans. Am. Geophys. Union* 90 (11).
- Prange, M., Lohmann, G., 2003. Effects of mid-Holocene river runoff on the Arctic ocean/sea-ice system: a numerical model study. *Holocene* 13 (3), 335–342. <https://doi.org/10.1191/0959683603hl626rp>.
- Rigor, I., 2015. Compiled by Polar Science Center 2002, IABP Drifting Buoy Pressure, Temperature, Position, and Interpolated Ice Velocity, Version 1. Subset C. NSIDC: National Snow and Ice Data Center, Boulder, Colorado USA.
- Rigor, I., Wallace, J., 2004. Variations in the age of Arctic sea-ice and summer sea-ice extent. *Geophys. Res. Lett.* 31 (L09401), 1–4.
- Rigor, I., Wallace, J., Colony, R., 2002. Response of sea ice to the arctic oscillation. *J. Clim.* 15, 2648–2663.
- Rotstayn, L.D., Collier, M.A., Dix, M.R., Feng, Y., Gordon, H.B., O'Farrell, S.P., Smith, I.N., Syktus, J., 2010. Improved simulation of Australian climate and ENSO-related rainfall variability in a global climate model with an interactive aerosol treatment. *Int. J. Climatol.* 30 (7), 1067–1088. <https://doi.org/10.1002/joc.1952>.
- Sachs, H., Webb, T., Clark, D., 1977. Paleocological transfer functions. *Annu. Rev. Earth Planet. Sci.* 5, 159–178.
- Schmidt, G.A., Kelley, M., Nazarenko, L., Ruedy, R., Russell, G.L., Aleinov, I., Bauer, M., Bauer, S.E., Bhat, M.K., Bleck, R., Canuto, V., Chen, Y.-H., Cheng, Y., Clune, T.L., Del Genio, A., de Fainchtein, R., Faluvegi, G., Hansen, J.E., Healy, R.J., Kiang, N.Y., Koch, D., Lacis, A.A., LeGrande, A.N., Lerner, J., Lo, K.K., Matthews, E.E., Menon, S., Miller, R.L., Oinas, V., Olosio, A.O., Perlwitz, J.P., Puma, M.J., Putman, W.M., Rind, D., Romanou, A., Sato, M., Shindell, D.T., Sun, S., Syed, R.A., Tausnev, N., Tsigaridis, K., Unger, N., Voulgarakis, A., Yao, M.-S., Zhang, J., 2014. Configuration and assessment of the GISS ModelE2 contributions to the CMIP5 archive. *J. Adv. Model. Earth Syst.* 6 (1), 141–184. <https://doi.org/10.1002/2013MS000265>.
- Stevens, B., Giorgetta, M., Esch, M., Mauritsen, T., Crueger, T., Rast, S., Salzmann, M., Schmidt, H., Bader, J., Block, K., Brokopf, R., Fast, I., Kinne, S., Kornbluh, L., Lohmann, U., Pincus, R., Reichler, T., Roeckner, E., 2013. Atmospheric component of the MPI-M earth system model: ECHAM6. *J. Adv. Model. Earth Syst.* 5 (2), 146–172. <https://doi.org/10.1002/jame.20015>.
- Thorndike, A., 1984. The Geophysics of Sea Ice: Chapitre 7: Kinematic of Sea Ice. Springer US.
- Vancoppenolle, M., Fichefet, T., Goosse, H., Bouillon, S., Madec, G., Morales Maqueda, M., 2009. Simulating the mass balance salinity of Arctic and Antarctic sea ice. I. Model description and validation. *Ocean. Model.* 27, 33–53. <https://doi.org/10.1016/j.ocemod.2008.10.005>.
- Voldoire, A., Sanchez-Gomez, E., Salas y Méria, D., Decharme, B., Cassou, C., Sénési, S., Valcke, S., Beau, I., Alias, A., Chevallier, M., Déqué, M., Deshayes, J., Douville, H., Fernandez, E., Madec, G., Maisonnave, E., Moine, M.-P., Planton, S., Saint-Martin, D., Szopa, S., Tyteca, S., Alkama, R., Belamari, S., Braun, A., Coquart, L., Chauvin, F., 2013. The CNRM-CM5.1 global climate model: description and basic evaluation. *Clim. Dyn.* 40 (9), 2091–2121. <https://doi.org/10.1007/s00382-011-1259-y>.
- Wadhams, P., 2000. Ice in the Ocean. Taylor & Francis.
- Wheeler, R., Alix, C., 2004. Economic and Cultural Significance of Driftwood in Coastal Communities of Southwest Alaska. Technical Report. University of Alaska Fairbanks.